Chinese Journal of Chemical Engineering 85 (2025) 260–269

Contents lists available at ScienceDirect

Chinese Journal of Chemical Engineering

journal homepage: www.elsevier.com/locate/CJChE

Full Length Article

Characterization of gaseous products and activated chars from pyrolysis of sewage sludge in the presence of activating agent

Yuwen Zhu , Jian Liu , Ting Li , Xinrui Su *, Qian Dai , Chang Xu , Xuening Zhao , Hanqiao Liu

School of Energy and Safety Engineering, Tianjin Chengjian University, Tianjin 300384, China

ARTICLE INFO

Article history:
Received 23 January 2025
Received in revised form
29 March 2025
Accepted 13 April 2025
Available online 13 May 2025

Keywords:
Sewage sludge
Pyrolysis temperature
Activating agent
Pyrolysis gas
Activated char

ABSTRACT

Sewage sludge (SS) and SS impregnated with activating agents ($ZnCl_2$ and KOH) were pyrolyzed in a fixed-bed reactor to produce gaseous fuel and activated char. The effects of heating rate, pyrolysis temperature and activator type on gas yields, pore structure and adsorption properties of activated char were systematically studied. The results demonstrated that increasing the pyrolysis temperature from 450 °C to 850 °C proportionally enhanced H_2 and CO yields from the rapid pyrolysis of SS, while CH_4 yield showed minimal variation between 650 °C and 850 °C. $ZnCl_2$ notably increased the CO yield, reaching 71.9 $ml \cdot g^{-1}$ at 850 °C, but caused a marked reduction in CH_4 yield under the tested conditions. Similarly, KOH promoted CO yield at 750 °C and 850 °C, with minimal impact on CH_4 production. Both activators facilitated higher H_2 yields in the range of 450–550 °C, while the maximum H_2 yield (109.8 $ml \cdot g^{-1}$) was observed at 850 °C in the absence of activator. The activated char derived from $ZnCl_2$-assisted pyrolysis exhibited well-developed micro- and mesopore structures, with specific surface areas ranging from 188.2 to 54.1 $m^2 \cdot g^{-1}$ across pyrolysis temperatures of 450–850 °C. When evaluated as adsorbents for methylene blue removal, activated char with greater specific surface area and total pore volume exhibited superior adsorption capacity. The adsorption process was well-described by the pseudo-second-order kinetic model.

1. Introduction

Sewage sludge (SS) generated from wastewater treatment processes is a highly heterogeneous body, including microorganisms, undegraded organic matter, inorganic impurities and water [1,2], which could pose a threat to the ecological environment and human health, if not properly treated or disposed of. With the rapid urbanization occurring in many regions globally, the generation of SS has increased substantially. Current SS disposal methods primarily include landfilling, agricultural use and incineration [3,4], while these methods have some limitations, *e.g.,* requiring vast areas or having some unfavorable environmental impacts [5,6]. Because of its high content of organic matters, SS can be used as raw material to produce fuels and carbonaceous adsorbents. Pyrolysis, as a thermochemical method with the oxygen free, offers a viable alternative for converting SS into valuable products, such as combustible gas, bio-oil and activated char [7–9].

Development of pyrolysis process and its technology could be a promising option for sludge reduction and energy production [10]. Inguanzo *et al.* [11] demonstrated that both the oil and gas derived from SS pyrolysis possessed relatively high heating values, comparable to some traditional fuels. Chang *et al.* [12] showed that the combined energy output from pyrolysis oils and gases could nearly sustain the energy demands of the process itself. Chun *et al.* [13] highlighted that pyrolysis gas could achieve a higher heating value of up to 10107 $kJ \cdot m^{-1}$, while the specific area of the activated char reached 40.1 $m^2 \cdot g^{-1}$.

Activated char is also a primary product of SS pyrolysis. However, it is difficult to achieve a specific surface area higher than 200 $m^2 \cdot g^{-1}$ directly by pyrolysis of SS [14,15]. In general, activated chars with higher porosities can be prepared by chemical activation, which refers to the impregnation of SS with chemical agents such as ZnCl, KOH, H_2SO_4 and H_3PO_4. $ZnCl_2$ is a dehydration reagent that induces the charring and aromatization of carbonaceous materials during pyrolysis [16]. KOH, which is a very effective

* Corresponding author.
E-mail address: 270648580@qq.com (X. Su).

https://doi.org/10.1016/j.cjche.2025.04.008

activating agent, reacts with carbon through multistep redox reactions [17]. In both cases, the obtained activated char has a developed porous structure that allows for its use as an adsorbent. Chen *et al.* [18] indicated that pyrolysis of SS impregnated with $ZnCl_2$ and KOH could be an energy-saving approach for producing activated char suitable for de-NO_x applications. Li *et al.* [19] prepared activated chars from SS using ZnCl, H_2SO_4 and KOH as activators, respectively, and observed superior H_2S adsorption performance in chars activated with $ZnCl_2$ and KOH.

Many studies have concentrated on recycling SS by making adsorbents for dye wastewater treatment. Methylene blue (MB), a basic dye, is widely used in the textile, printing, leather, cosmetics, and food industries as a raw coloring agent. Li *et al.* [20] reported a method for preparing SS activated carbon by activating pyrolysis char with ZnCl, and the maximum uptake of MB was 95.3 $mg \cdot g^{-1}$. Rozada *et al.* [16] demonstrated that SS activated carbon, using $ZnCl_2$ as activator, exhibited an MB adsorption capacity of 139.4 $mg \cdot g^{-1}$, significantly surpassing that of H_2SO_4-activated carbon. Mahapatra *et al.* [21] conducted a comparative evaluation of dye adsorption capacity between commercial and synthesized rubber sludge-derived activated carbon, and found the kinetics of MB removal by synthesized activated carbon was faster than the commercial one. The preparation of activated carbon from SS would not only transform solid waste into a valuable adsorbent but also have the potential to replace commercial adsorbents for wastewater treatment.

In the light of previous research, the primary objective of this study was to improve the resource utilization of SS. By conducting SS pyrolysis in the presence of activating agent, the resulting gas product can serve as a fuel directly, while the solid product can also function effectively as an adsorbent. The study provided a simple method for integrating sludge disposal, energy recovery, adsorbent preparation and wastewater treatment. The pyrolysis characteristics of SS in the presence of $ZnCl_2$ or KOH were investigated with the dual objectives of recovering gas and char products. The effects of pyrolysis conditions, including heating rate and final temperature, as well as activating agents on the main characteristics of gas and activated char were systematically investigated in a laboratory-scale tubular furnace. To assess the potential applications of the resulting activated char, its adsorption behavior was evaluated using MB.

2. Experimental Methods

2.1. Experimental material

The dewatered SS was obtained from the Xianyang Road Wastewater Treatment Plant in Tianjin, China. The proximate and ultimate analysis of the SS was shown in Table 1. The SS had a low fixed carbon (FC_{ad}) content of 5.9%, a volatile matter (V_{ad}) content of 48.5%, and a heating value (Q_{net}) of 11.2 $MJ \cdot kg^{-1}$.

The SS was dried in an electronic oven at 100 °C for 24 h. The dried sludge was then powdered and sieved to a size range of 0.125–0.250 mm. Analytically pure $ZnCl_2$ and KOH, using as activating agents, were impregnated into the SS. 20 g of dried SS was immersed in 60 ml of 3 $mol \cdot L^{-1}$ $ZnCl_2$ or KOH solution, mixed at room temperature for 24 h, and subsequently dried in an oven at 100 °C for 24 h. The impregnated sludge samples were denoted as SS-$ZnCl_2$-3 and SS-KOH-, respectively.

2.2. Experimental equipment and procedure

The prepared sludge samples were pyrolyzed at different heating rates and final temperatures in a horizontal tube furnace. During the temperature-programmed pyrolysis, 10 g of sample was evenly spread in a corundum boat and placed at the center of the reactor tube (50 mm inner diameter and 400 mm length). The sample was heated from room temperature to 950 °C at a rate of 8 $°C \cdot min^{-1}$ under a N_2 flow of 400 $ml \cdot min^{-1}$. During the above process, pyrolysis gases, including H, CO, CH_4 and CO, were continuously detected and recorded at 10 °C intervals using a gas analyzer (GE-MP, Gechee, China). During gas sampling, tar was removed *via* three ethyl alcohol absorption bottles and a cotton filter to protect the gas analyzer.

For the rapid pyrolysis experiments, the reactor was purged with a constant N_2 flow (400 $ml \cdot min^{-1}$) to maintain an inert atmosphere. When the heating zone of furnace reached the desired reaction temperature (450, 550, 650, 750 or 850 °C), 5 g of sludge sample in a corundum boat was quickly put into the reactor. Pyrolysis proceeded until no further gases were detected, with gas monitoring performed every 30 s. The resulting char was cooled to room temperature under N. The obtained activated char was washed three times with 1 $mol \cdot L^{-1}$ HCl solution to eliminate the remains of the chemical activator [16], followed by deionized water rinses until the supernatant reached neutral pH. Finally, the activated char was dried at 100 °C.

The activated chars obtained from temperature-programmed pyrolysis were designated as SCP, SCP-$ZnCl_2$-3 and SCP-KOH-, respectively, where "3" represents the use of a 3 $mol \cdot L^{-1}$ $ZnCl_2$ or KOH solution for impregnating the sludge. Meanwhile, the activated chars derived from fast pyrolysis were labeled as SCF-$ZnCl_2$-(temperature) and SCF-KOH-(temperature). For instance, SCF-$ZnCl_2$-850 refers to the activated char produced from $ZnCl_2$-impregnated SS at a pyrolysis temperature of 850 °C.

2.3. Characterization of sludge samples and activated chars

The pyrolysis reactivity of sludge samples was measured using a thermogravimetric analyzer (HCT-4, Henven, China). Approximately 20 mg of sample was heated to 950 °C at a rate of 8 $°C \cdot min^{-1}$ under a N_2 flow of 50 $ml \cdot min^{-1}$. The porous structure parameters of activated chars were determined *via* nitrogen adsorption–desorption analysis (JW-BK 200C, JWGB, China) at −196 °C. Before analysis, the activated chars were degassed at 200 °C under vacuum for 8 h. The specific surface area was calculated using the Brunauer-Emmett-Teller (BET) equation [22]. The mesopore volume and pore size distributions were calculated by applying the Barrett-Joyner and Halenda (BJH) method [23]. The total pore volume was calculated from the N_2 adsorbed amount at a relative pressure (P/P_0) of 0.99. The surface morphology of activated chars was observed using scanning electron microscopy (SEM, JSM-6360LA, JEOL, Japan). The types of surface functional groups were

Table 1
Proximate and ultimate analysis of SS.

Proximate analysis/% (mass)					Ultimate analysis/% (mass)				
M_{ad}	V_{ad}	FC_{ad}	A_{ad}	$Q_{net}/MJ \cdot kg^{-1}$	C_{ad}	H_{ad}	O_{ad}*	N_{ad}	S_{ad}
6.5	48.5	5.9	39.1	11.2	26.0	2.1	19.9	3.5	2.9

* By difference.

identified by Fourier transform infrared (FTIR) spectroscopy (Magna-IR 560 E.S.P, Nicolet, USA) in the range of 4000–500 cm^{-1} with a resolution of 4 cm^{-1}, using KBr pellets containing approximately 0.5% (mass) sample.

2.4. MB adsorption experiment

The adsorption performance of activated chars was evaluated using MB as an adsorbate by batch adsorption method [24]. Typically, 20 mg of activated char was mixed with 500 ml of MB solution with initial concentration of 10 $mg \cdot L^{-1}$ under magnetic stirring of 400 $r \cdot min^{-1}$ at 30 °C. The absorbance of the MB solution was measured at a wavelength of 664 nm using a UV–visible spectrophotometer (UV759CRT, Yoke, China).

The adsorption capacity (Q_e) of MB was calculated using Eq. (1):

$$Q_e = \frac{(C_0 - C) \cdot V}{1000 \cdot M} \quad (1)$$

where Q_e is the MB adsorption capacity ($mg \cdot g^{-1}$), V is the solution volume (ml), M is the mass of adsorbent (g), C_0 is the initial MB concentration ($mg \cdot L^{-1}$), and C is the final MB concentration ($mg \cdot L^{-1}$).

3. Results and Discussion

3.1. Thermogravimetric analysis

The thermogravimetric (TG) method was used to characterize the pyrolysis behavior of sludge samples (SS, SS-$ZnCl_2$-3 and SS-KOH-3). The TG curves in Fig. 1(a) illustrate the mass loss of sludge samples as a function of temperature during pyrolysis. From room temperature to 400 °C, SS-$ZnCl_2$-3 and SS-KOH-3 presented similar mass loss, both lower than that of SS. Between 400 and 900 °C, SS-$ZnCl_2$-3 experienced the highest mass loss up to 4.7%, followed by SS-KOH-, while SS showed the lowest mass loss of 25.8%. The total mass loss at 900 °C was 6.8% for SS-$ZnCl_2$-, 54.9% for SS, and 47.2% for SS-KOH-.

The differential thermogravimetric (DTG) curves in Fig. 1(b) reveal the mass loss rate during pyrolysis. The small peaks below 150 °C were evaporation of moisture in sludge samples, while the intense peaks within 180–400 °C were attributed to the depolymerization of organic matter. SS exhibited an obviously higher mass loss rate (0.19%·°C^{-1}) than SS-KOH-3 (0.14%·°C^{-1}) and SS-$ZnCl_2$-3 (0.11%·°C^{-1}). When the temperature was higher than 400 °C, two small peaks were observed for SS at 430 °C and 810 °C, whereas SS-$ZnCl_2$-3 and SS-KOH-3 showed single peaks at 529 °C and 685 °C, respectively. The mass loss beyond 400 °C was primarily due to the decomposition of residual organic volatiles and inorganic substances [25,26]. Furthermore, SS-$ZnCl_2$-3 presented a higher mass loss rate and a lower decomposition temperature, indicating that $ZnCl_2$ in sludge could significantly promote the decomposition process.

3.2. Emission characteristics of pyrolysis gas

The temperature-programmed pyrolysis of SS, SS-$ZnCl_2$-3 and SS-KOH-3 in the range from 200 °C to 950 °C revealed significant effects of activating agent and temperature on the release of pyrolysis gases (H, CO, CH_4 and CO_2), as shown in Fig. 2.

As illustrated in Fig. 2(a), H_2 was released continuously from 350 °C to 950 °C during SS pyrolysis. The presence of $ZnCl_2$ and KOH significantly enhanced H_2 content, and shifted the emission range to 300–700 °C. For SS-$ZnCl_2$-, H_2 emission began to rise sharply at temperature above 300 °C, and reached a maximum level of 15.6% at approximately 400 °C. For SS-KOH-, H_2 was released above 360 °C, and rapidly reached its peak content of 11.5% at 440 °C. The above results suggested that $ZnCl_2$ and KOH promoted H_2 release in the range of 350–500 °C. From Fig. 2(b), CO was released from SS pyrolysis above 670 °C, reaching its peaks at 740 °C and 940 °C, respectively. In contrast, CO released from SS-KOH-3 highly increased with peak content of 11.3%, and the temperature reduced to the range of 600–750 °C. SS-$ZnCl_2$-3 exhibited significant CO release between 340°C and 440 °C, indicating that $ZnCl_2$ facilitated CO emission at lower temperatures. As shown in Fig. 2(c), CH_4 emissions occurred within 350–500 °C for all samples. However, the activating agents had a great influence on the concentration of CH_4. The maximum level of CH_4 released from SS-KOH-3 was higher than that of SS, reaching its peak content of 9.8%, while the level of CH_4 was drastically reduced during the SS-$ZnCl_2$-3 pyrolysis and the maximum content was less than 3.0%. Fig. 2(d) showed CO_2 release was much lower compared to other gases. The emission of CO_2 was lower than 500 °C, which was mainly caused by the decarboxylation reaction. In comparison, the level of CO_2 was enhanced in the presence of KOH, while it was largely inhibited during SS-$ZnCl_2$-3 pyrolysis.

Based on the emission characteristics of gases from the temperature-programmed pyrolysis of SS, SS-$ZnCl_2$-3 and SS-KOH-,

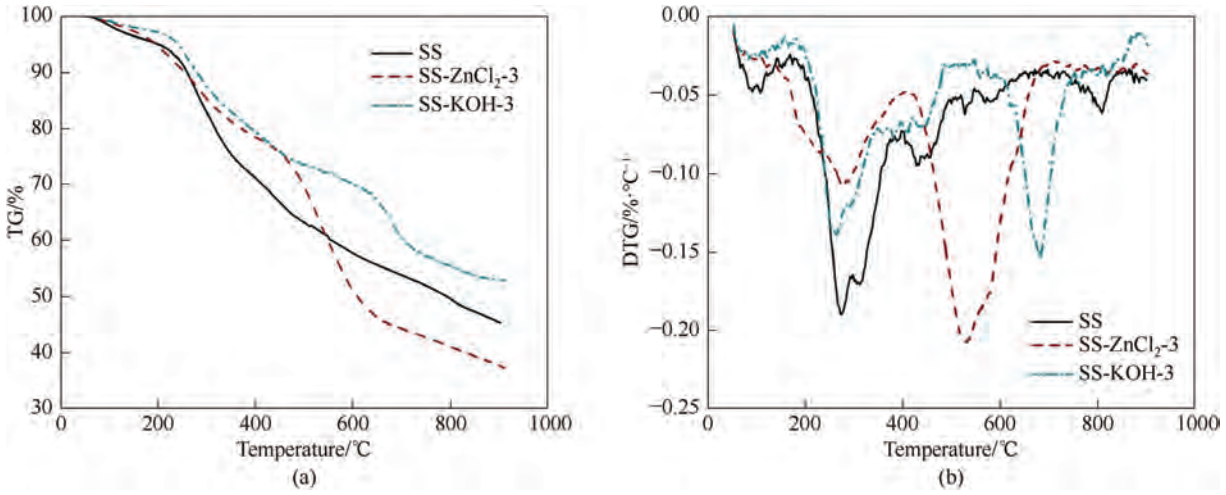

Fig. 1. TG and DTG curves of various sludge samples (SS, SS-$ZnCl_2$-3 and SS-KOH-3) under simulated pyrolysis. (a) TG curves, (b) DTG curves.

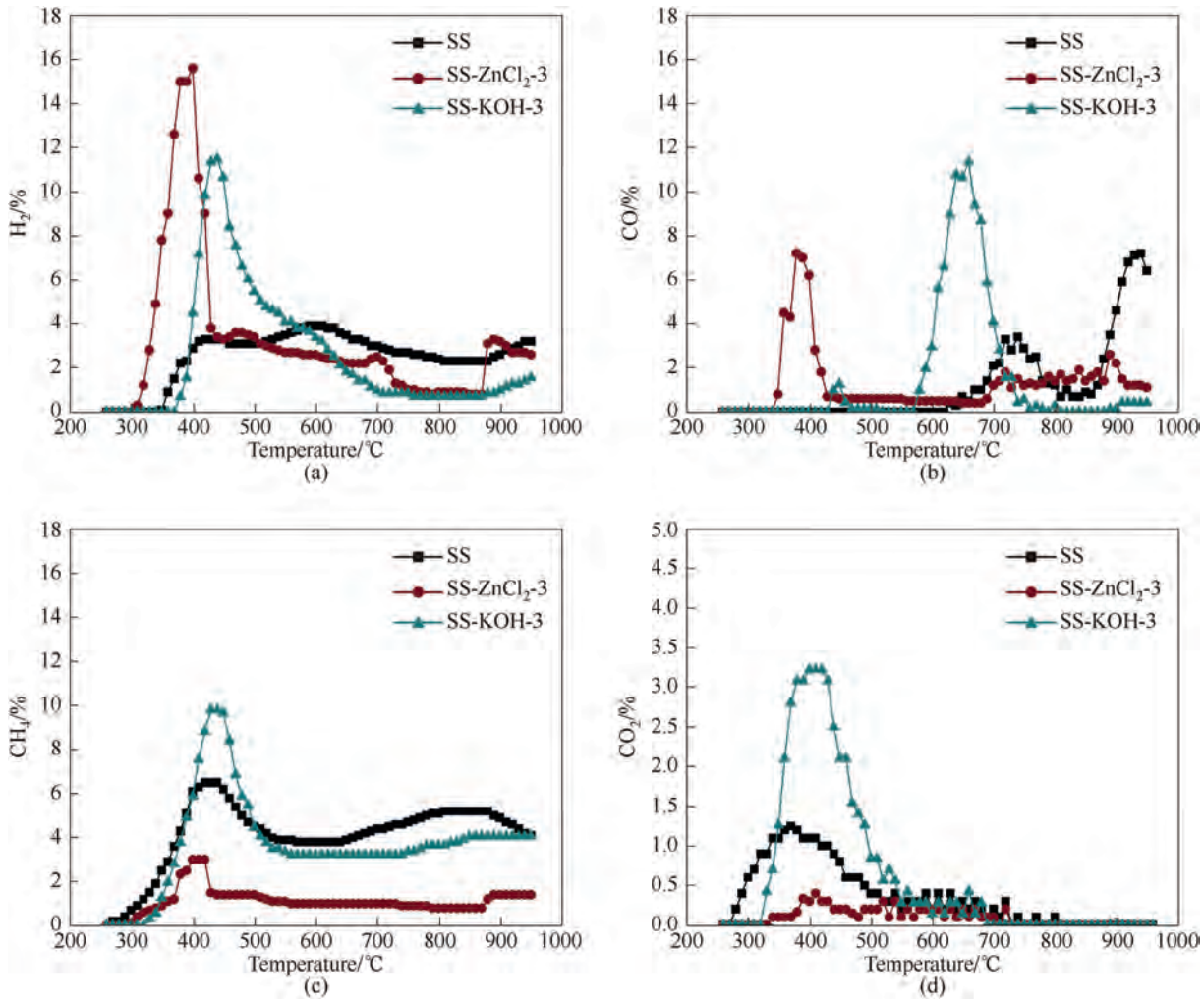

Fig. 2. Emission profiles of pyrolysis gases from temperature-programmed pyrolysis of SS, SS-$ZnCl_2$-3 and SS-KOH-. (a) H, (b) CO, (c) CH_4, (d) CO.

the gas yields from fast pyrolysis at different temperatures (450–850 °C) were summarized in Fig. 3.

As shown in Fig. 3(a), the H_2 yield was found to improve proportionally with increasing temperature. H_2 yields from SS-$ZnCl_2$-3 and SS-KOH-3 pyrolysis were higher compared to SS pyrolysis at 450–550 °C. Combined with the emission profile of H_2 from temperature-programmed pyrolysis, both $ZnCl_2$ and KOH in sludge could highly promote the level of H_2 below 500 °C, which led to a higher H_2 production at lower temperatures (450 °C and 550 °C). However, when the pyrolysis temperature was higher than 650 °C, the maximum H_2 yield was obtained from SS, reaching 109.8 $ml \cdot g^{-1}$ at 850 °C. Similar to the H_2 yield, the temperature showed marked positive influence on CO production from the fast pyrolysis of the three samples as shown in Fig. 3(b). CO production was highest for SS-$ZnCl_2$-3 in the range of 450°C–850 °C, peaking at 71.9 $ml \cdot g^{-1}$. For SS-KOH-, CO yield was the lowest among the sludge samples across 450–650 °C. However, when the temperature reached 750 °C and 850 °C, KOH could promote CO yield, and the maximum value of 75.6 $ml \cdot g^{-1}$ was achieved at 850 °C. As shown in Fig. 3(c), CH_4 yield increased with pyrolysis temperature up to 650 °C and plateaued at higher temperatures. In the case of KOH-impregnated sludge, the CH_4 yields were slightly higher than those of SS at 450 °C and 550 °C. By contrast, CH_4 yields from SS-$ZnCl_2$-3 were lowest throughout the temperature range, which indicated the inhibition of the CH_4 release by ZnCl, according well with the temperature-programmed pyrolysis of SS-$ZnCl_2$-3 in Fig. 2(c). From Fig. 3(d), the total yield of the above combustible gases improved proportionally with increasing temperature. The total yields of gases from fast pyrolysis of SS and SS-KOH-3 had little difference, while that of SS-$ZnCl_2$-3 was the lowest except 450 °C.

3.3. Properties of activated char

The activated chars were obtained from SS pyrolysis in the presence of $ZnCl_2$ and KOH. The characteristics of the prepared activated chars, including surface morphology, pore structure and functional group, were investigated.

Fig. 4 (a)–(c) showed the SEM images of activated chars from temperature-programmed pyrolysis. From Fig. 4 (a), it can be observed that SCP from SS pyrolysis exhibited a smooth surface with some shallow pores (diameters of 1–2 μm). In contrast, SCP-KOH-3 and SCP-$ZnCl_2$-3 had relatively rough and eroded surfaces with larger pores (2–5 μm) distribution. Fig. 4 (d)–(f) showed the images of chars from fast pyrolysis at 850 °C, which displayed more rough and porous surface due to increased gases release and destruction of char structure under the vigorous reaction conditions.

Fig. 5 showed the N_2 adsorption–desorption isotherms and pore size distributions of activated chars. As shown in Fig. 5 (a), SCP derived from the SS had the lowest N_2 adsorption quantity. By contrast, the N_2 adsorption quantities of SCP-$ZnCl_2$-3 and SCP-

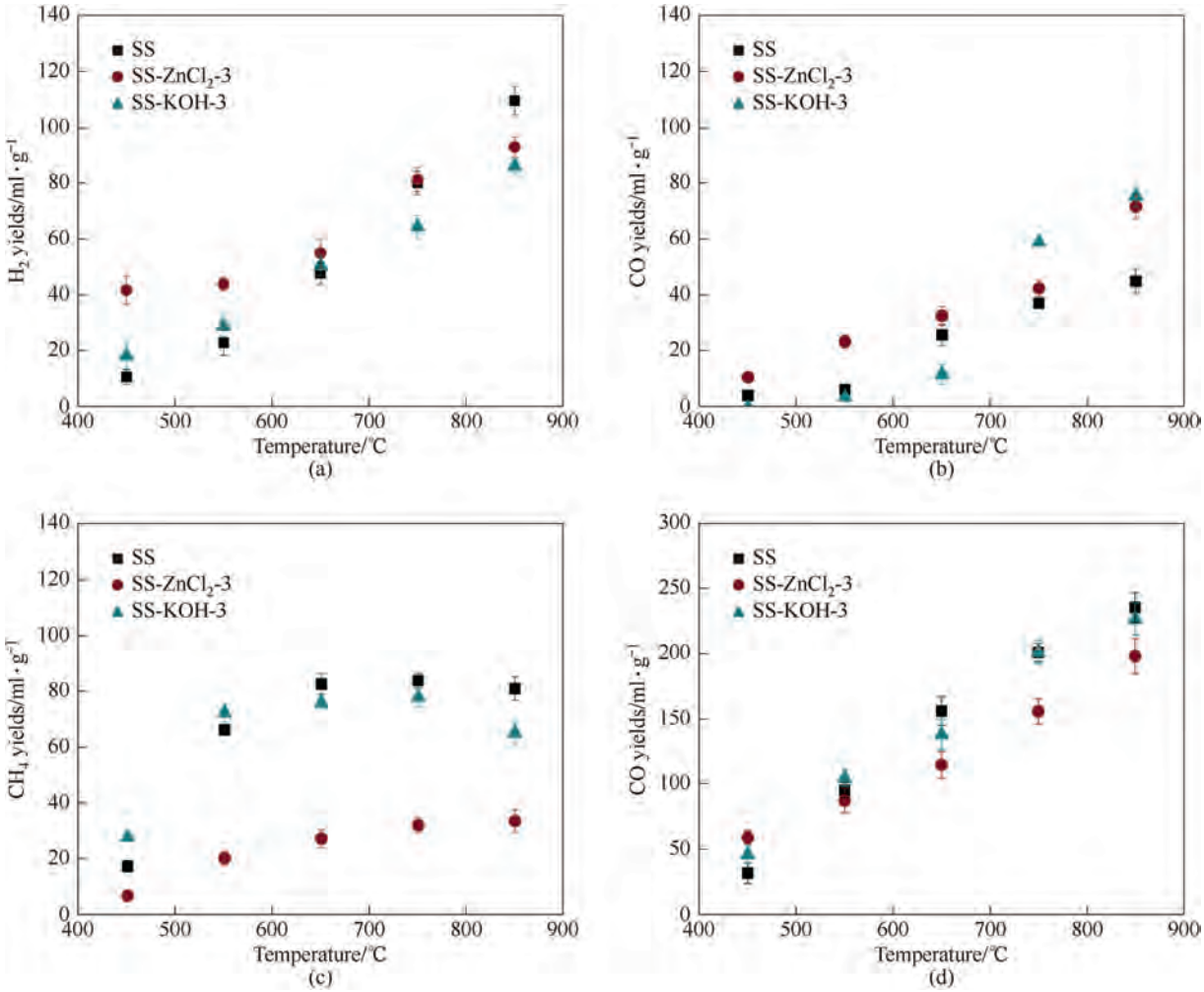

Fig. 3. Evolution of combustible gases yields from fast pyrolysis of SS, SS-$ZnCl_2$-3 and SS-KOH-3 at different temperatures: (a) H, (b) CO, (c) CH_4 and (d) total yields of H, CO and CH_4.

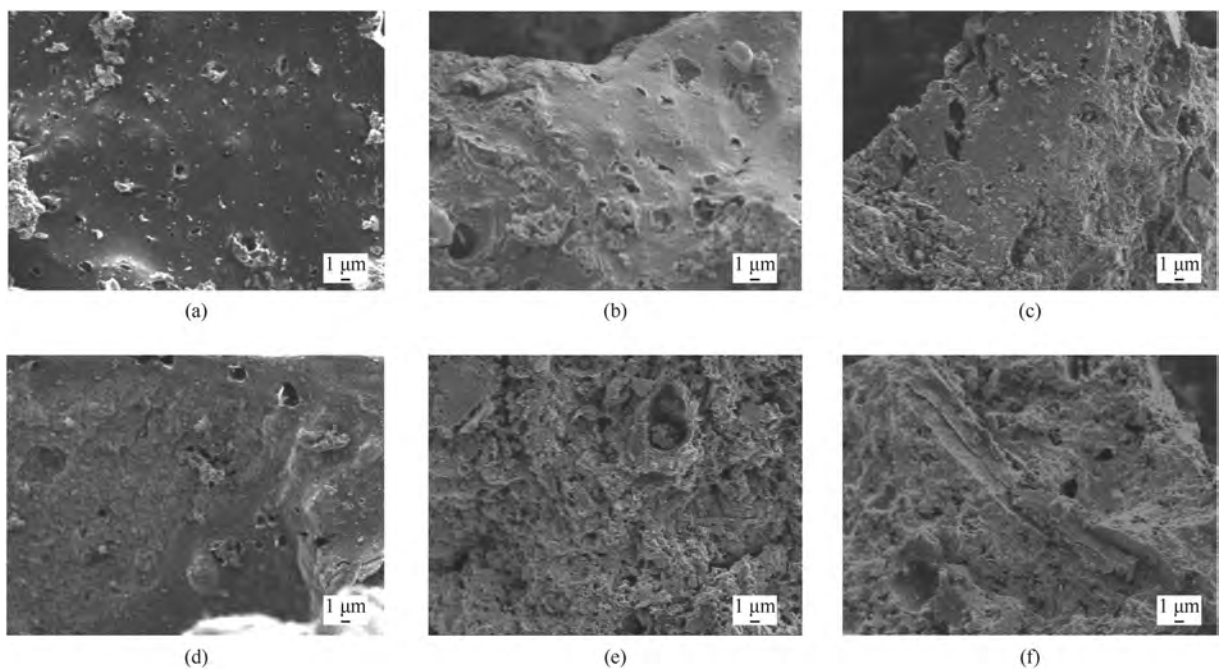

Fig. 4. SEM images of activated chars at 3000× magnification. Activated chars from temperature-programmed pyrolysis: (a) SCP, (b) SCP-KOH-, (c) SCP-$ZnCl_2$-. Activated chars from fast pyrolysis: (d) SCF-850, (e) SCF-KOH-850, (f) SCF-$ZnCl_2$-850.

KOH-3 increased obviously with increasing relative pressure (P/P_0). More specifically, SCP-$ZnCl_2$-3 had the highest N_2 adsorption amounts which increased abruptly at $P/P_0 < 0.1$ and had a significant growth at high P/P_0 region, indicating fully developed micro- and mesopore structures. The hysteretic loop also appeared in SCP-KOH-3 and indicated the existence of mesopores. The corresponding pore structure parameters of activated chars were summarized in Table 2. As can be seen, SCP-$ZnCl_2$-3 exhibited the highest BET surface area (S_{BET}) and total pore volume (V_{tot}) up to 458.3 $m^2 \cdot g^{-1}$ and 0.442 $cm^3 \cdot g^{-1}$, respectively, followed by SCP-KOH-, while SCP showed much lower values of 89.2 $m^2 \cdot g^{-1}$ and 0.104 $cm^3 \cdot g^{-1}$, respectively. The above activated chars had narrow mesopore size distributions which centered at 3–4 nm as shown in Fig. 5(b).

Table 2
Pore structure parameters of activated chars.

Samples	S_{BET}/ $m^2 \cdot g^{-1}$	V_{tot}/ $cm^3 \cdot g^{-1}$	V_{mic}/ $cm^3 \cdot g^{-1}$	V_{mes}/ $cm^3 \cdot g^{-1}$	V_{mes}/ V_{tot}	D_{mean}/ nm
SCP	89.2	0.104	0.006	0.098	0.942	1.67
SCP-KOH-3	318.2	0.274	0.069	0.205	0.745	0.17
SCP-$ZnCl_2$-3	458.3	0.442	0.185	0.257	0.569	0.44
SCF-$ZnCl_2$-450	339.5	0.417	0.158	0.259	0.621	0.28
SCF-$ZnCl_2$-650	54.1	0.539	0.243	0.296	0.549	0.65
SCF-$ZnCl_2$-850	188.2	0.262	0.080	0.182	0.695	0.74

Based on the fully developed pore structures of SCP-$ZnCl_2$-3 derived from $ZnCl_2$-impregnated SS, $ZnCl_2$ was chosen as the representative activating agent to discuss the roles of temperature in fast pyrolysis for porous structures. A set of activated chars from fast pyrolysis at 450, 650 and 850 °C were obtained. Fig. 5(c) showed the N_2 adsorption quantities of activated chars first increased and then decreased with increasing temperature. SCF-$ZnCl_2$-650 exhibited the highest N_2 adsorption amounts up to 276.3 $cm^3 \cdot g^{-1}$, while SCF-$ZnCl_2$-850 had the lowest amount of 18.7 $cm^3 \cdot g^{-1}$. The isotherms of activated chars all showed obvious loops at P/P_0 of 0.4–1.0, indicating the formation of mesopores in fast pyrolysis. As summarized in Table 2, the mesopore volumes (V_{mes}) of the above activated chars were in the range of 0.182–0.296 $cm^3 \cdot g^{-1}$. SCF-$ZnCl_2$-650 possessed the highest S_{BET} and V_{tot} up to 54.1 $m^2 \cdot g^{-1}$ and 0.539 $cm^3 \cdot g^{-1}$, respectively. However, higher temperature (850 °C) adversely affected pore structure development, leading to a low S_{BET} of 188.2 $m^2 \cdot g^{-1}$. As shown in Fig. 5(d), the mesopores mainly centered around 3–4 nm, and the mean pore diameters (D_{mean}) were about 2.74–3.65 nm.

The FTIR spectra of SCP, SCP-$ZnCl_2$-3 and SCP-KOH-3 were shown in Fig. 6 to evaluate the effects of activating agent on the surface chemical properties. It can be seen that the peak around 3436 cm^{-1} in the SCP spectra was corresponding to the stretching

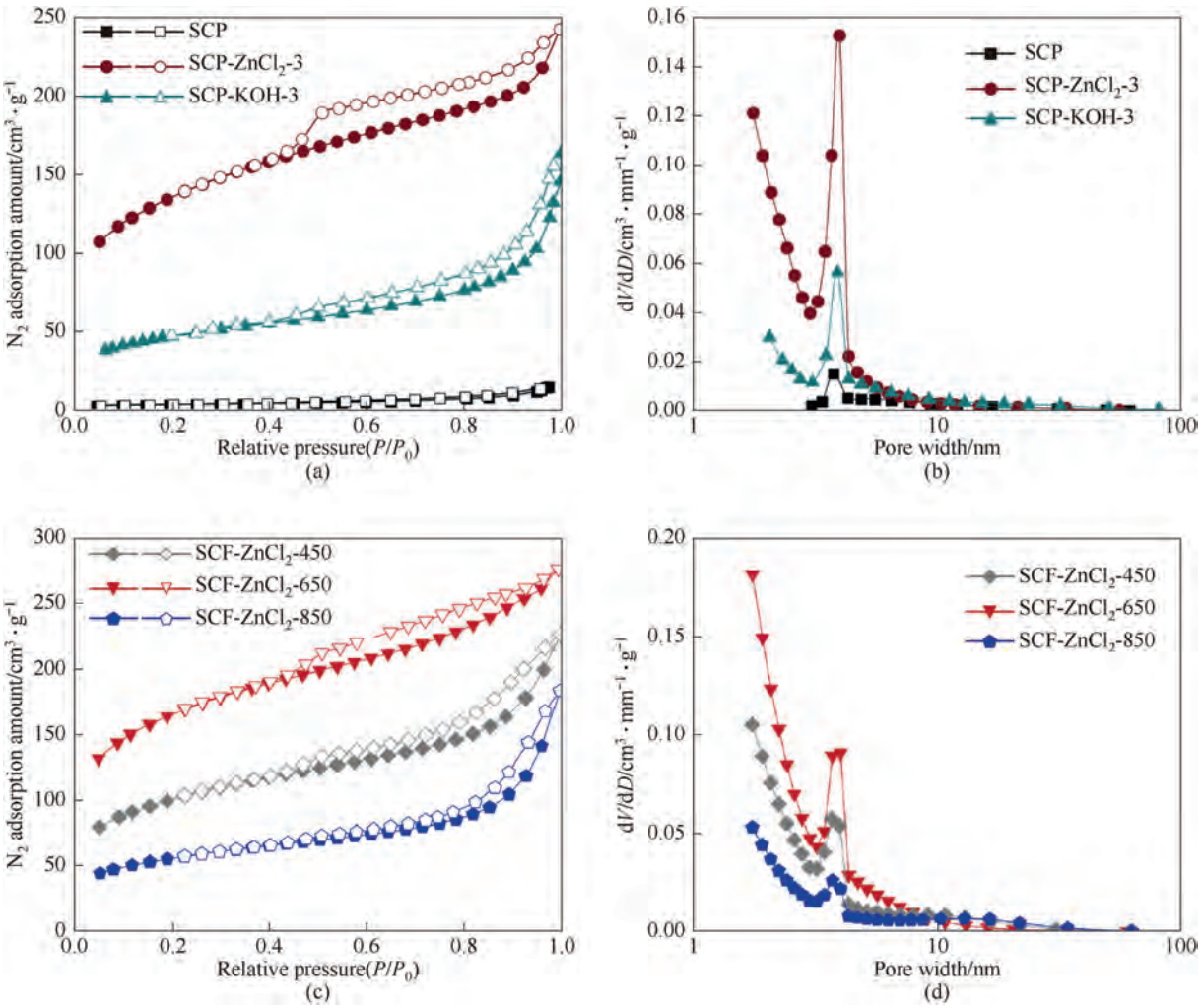

Fig. 5. Characterization of pore structures of activated chars: (a), (c) N_2 adsorption and desorption isotherms; (b), (d) Pore size distributions.

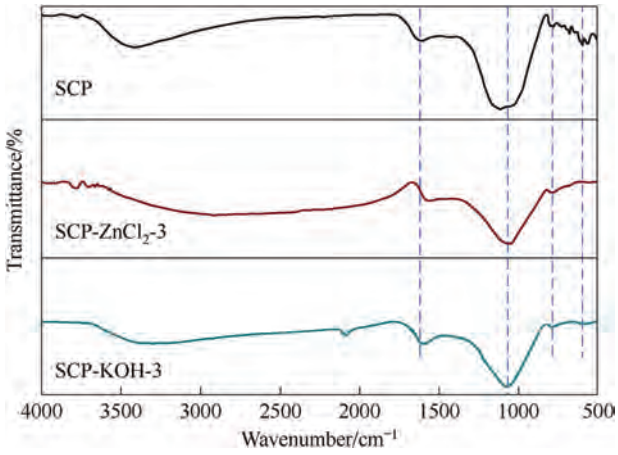

Fig. 6. FTIR spectra of sludge chars.

vibrations of hydroxyl, while in this range peak intensities of SCP-$ZnCl_2$-3 and SCP-KOH-3 were extremely low. The peaks around 1620 cm^{-1} were corresponding to the stretching vibration of C=O [27]. The broad, intense peaks appeared within the range of 1200–1100 cm^{-1} were assigned to C–O stretching vibration [28]. The peaks at 796 cm^{-1} were caused by C–H bending vibration [29], and the peaks were relatively strong in the SCP and SCP-$ZnCl_2$-3 spectra. The peaks at 700–650 cm^{-1} appeared in the SCP spectra may be assigned to skeletal vibrations, amine and amide groups [30], but those were not observed for chars with $ZnCl_2$ and KOH activation. As shown in Fig. 6, SCP-$ZnCl_2$-3 and SCP-KOH-3 had similar peak positions in FTIR spectra, indicating that type of activating agent had little impact on the functional group composition.

3.4. Adsorption of MB on activated char

MB, with a molecule diameter of 1.1–1.5 nm, was used as an indicator to evaluate the adsorption capacity of activated chars [31,32], as shown in Fig. 7. The adsorption curves of MB on SCP, SCP-$ZnCl_2$-3 and SCP-KOH-3 verse time were presented in Fig. 7(a). The MB adsorption amounts of SCP reached equilibrium within 50 min with saturated capacity of 50.2 $mg \cdot g^{-1}$, while the adsorption amounts of SCP-$ZnCl_2$-3 and SCP-KOH-3 increased with time and reached equilibrium after 105 min with capacities of 96.9 and 74.0 $mg \cdot g^{-1}$, respectively. Fig. 7(b) showed the time-dependent variation of MB adsorption on activated chars obtained from fast pyrolysis. SCF-$ZnCl_2$-650 exhibited superior adsorption performance compared to other chars, reaching equilibrium after 88 min

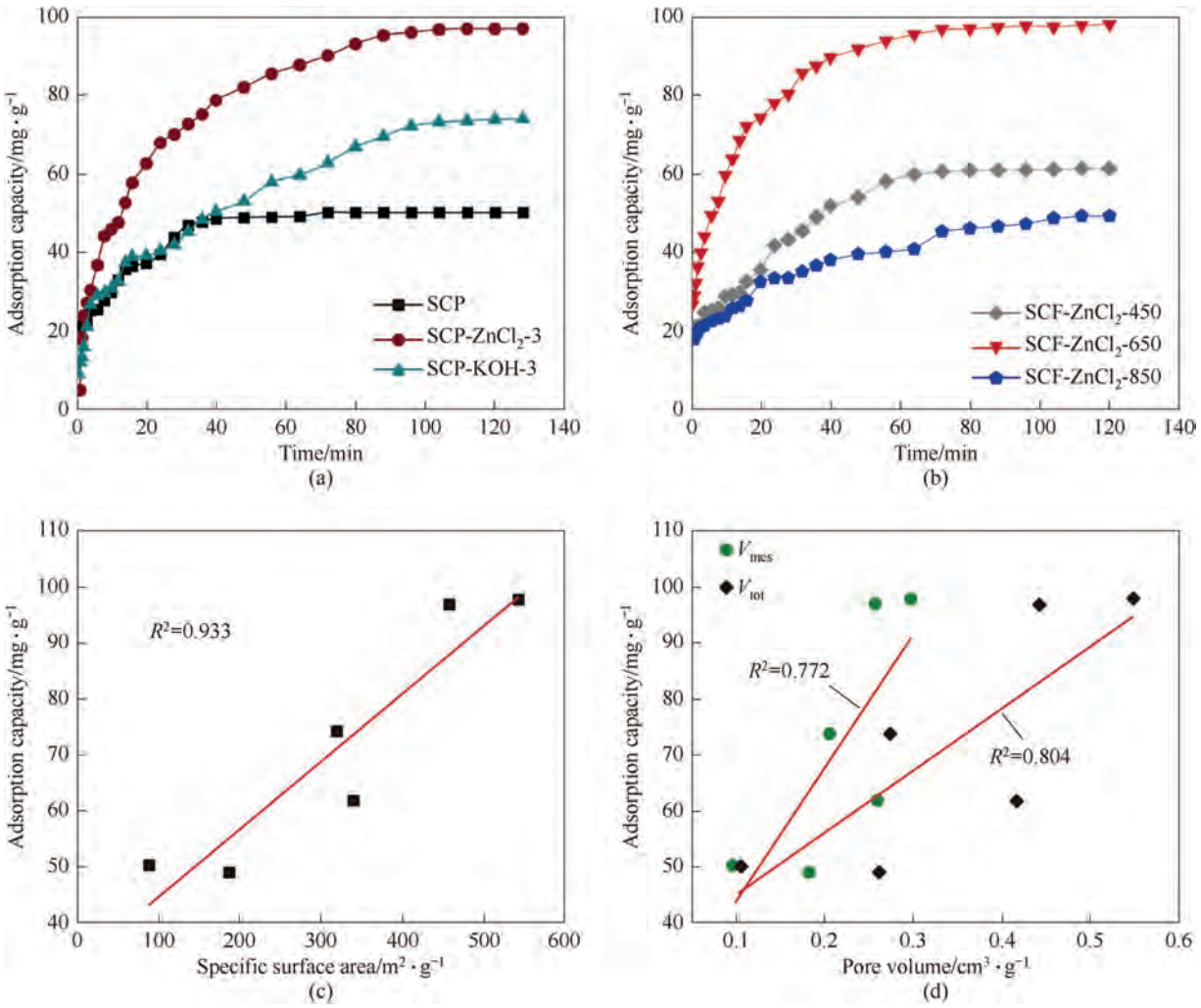

Fig. 7. MB adsorption capacities of activated chars: (a) activated chars from temperature-programmed pyrolysis, (b) activated chars from fast pyrolysis, (c) and (d) relationships between MB adsorption capacities and pore parameters.

Table 3
Kinetic parameters of MB adsorption on sludge chars.

Sludge chars	Q_e(exp.)/mg·g^{-1}	Pseudo-first-order kinetic			Pseudo-second-order kinetic		
		$k_1 \times 10^{-2}$/min^{-1}	Q_e(cal.)/mg·g^{-1}	R^2	$k_2 \times 10^{-2}$/min^{-1}	Q_e(cal.)/mg·g^{-1}	R^2
SCP	50.2	6.27	0.6	0.959	4.42	5.6	0.998
SCP-KOH-3	74.0	0.85	77.0	0.895	1.54	74.0	0.996
SCP-$ZnCl_2$-3	96.9	5.53	11.7	0.902	0.89	107.1	0.996
SCF-$ZnCl_2$-450	61.9	6.45	7.3	0.854	1.68	66.7	0.986
SCF-$ZnCl_2$-650	98.0	4.97	65.2	0.991	1.89	10.7	0.998
SCF-$ZnCl_2$-850	49.1	4.41	45.7	0.768	0.25	50.9	0.985

with an adsorption capacity of 98.0 mg·g^{-1}. It could be attributed to its larger specific surface area and pore volume, which provided more active sites for MB adsorption.

Considering the minor differences in surface functional groups, the MB uptake by the obtained activated char was primarily attributed to the pore structure parameters. The relationship between MB adsorption amounts and S_{BET} of activated chars was plotted in Fig. 7(c). The results showed a strong linear correlation ($R^2 = 0.933$), indicating that a larger S_{BET} contributed to improved adsorption performance by offering more adsorption sites [33]. Meanwhile, MB adsorption amounts increased with increasing V_{tot} and V_{mes}, as shown in Fig. 7(d). Notably, there was a better linear relationship between MB adsorption capacity and V_{tot} with higher R^2 value of 0.804, which illustrated V_{tot} played a more significant role in determining adsorption performance.

To further investigate the dynamics of MB adsorption on activated chars, the experimental data were fitted using the pseudo-first-order and pseudo-second-order kinetic models [34,35]. The pseudo-first-order model assumes that adsorption is primarily controlled by diffusion, with the reaction rate proportional to the amount of remaining adsorbate in the solution [36]. Its integral equation of linear form was as follows:

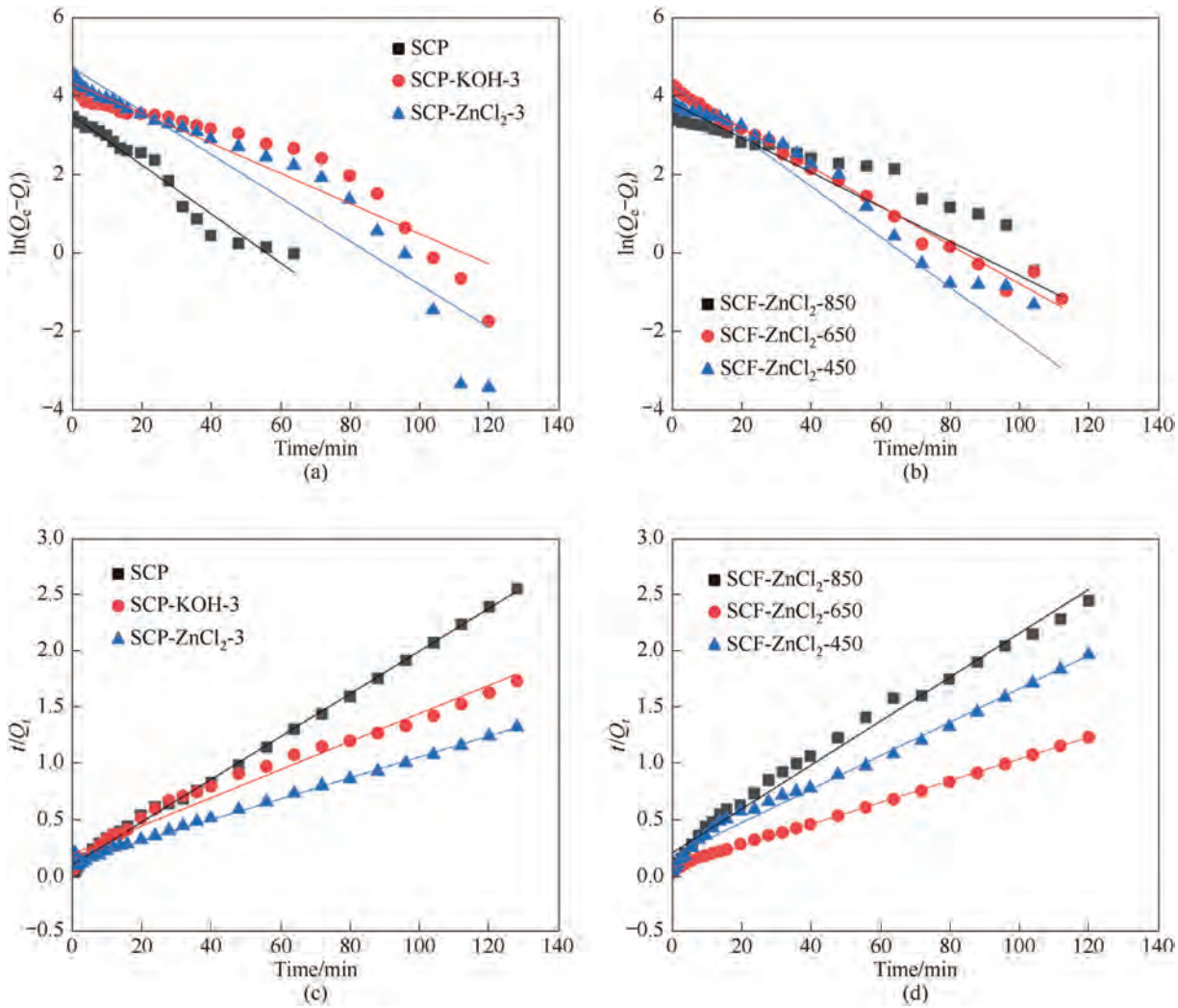

Fig. 8. Fitting results of pseudo-first-order model and pseudo-second-order model: (a) and (b) pseudo-first-order model, (c) and (d) pseudo-second-order model.

$$\ln(Q_e - Q_t) = \ln Q_e - k_1 t \quad (2)$$

where t is reaction time (min), Q_e represents the adsorption quantity of MB on activated chars at equilibrium ($mg \cdot g^{-1}$), Q_t is the adsorption capacity at t ($mg \cdot g^{-1}$), and k_1 represents the pseudo-first-order rate constant (min^{-1}).

The pseudo-second-order model assumes that adsorption process is mainly controlled by the chemical adsorption steps. The adsorption reaction rate constant is proportional to the square of the adsorbate concentration [37]. The linear expression was as follows:

$$\frac{t}{Q_t} = \frac{1}{k_2 Q_e^2} + \frac{t}{Q_e} \quad (3)$$

Where k_2 is the pseudo-second-order reaction rate constant ($mg \cdot g^{-1} \cdot min^{-1}$).

The fitting parameters were listed in Table 3 and the fitting results were displayed in Fig. 8. The equilibrium adsorption capacity (Q_e), k_1 and k_2 values were derived from the slopes and intercepts of the fitted lines. It can be seen from Fig. 8(a) and (b) that pseudo-first-order model effectively described the initial stage of MB adsorption, but failed to capture the features throughout the adsorption process. This was evident from the R^2 values, which ranged from 0.768 to 0.991, as shown in Table. The calculated (cal.) and experimental (exp.) values of Q_e showed significant difference, which further suggested that the pseudo-first-order model was inadequate for describing MB adsorption on activated chars. In contrast, the pseudo-second-order model exhibited better fitting results, with R^2 values exceeding 0.985 for all samples. The calculated values closely matched the experimental data, indicating that MB adsorption on sludge chars was better described by the pseudo-second-order model. It revealed that the process was predominantly controlled by chemisorption mechanisms rather than mass transfer from the bulk solution to the adsorbent surface. Among the activated chars from fast pyrolysis, SCF-$ZnCl_2$-850 exhibited the most rapid adsorption kinetics, as evidenced by its superior k_2 value, followed by SCF-$ZnCl_2$-650. On the other hand, for activated chars from temperature-programmed pyrolysis, SCP displayed the highest k_2 value across all investigated samples.

4. Conclusions

In summary, the characteristics of gas and activated char derived from SS pyrolysis in the presence of activating agents (KOH and $ZnCl_2$) were investigated. In fast pyrolysis, $ZnCl_2$ in sludge could promote CO production across all tested temperatures and highly enhance H_2 production at lower temperatures (450 and 550 °C), while simultaneously inhibiting CH_4 release. KOH in sludge could lead to a higher H_2 production at 450–550 °C and a higher CO production at 750–850 °C. The maximum total yield of H, CO and CH_4 was 235.9 $ml \cdot g^{-1}$ under the condition of SS fast pyrolysis at 850 °C. $ZnCl_2$ showed a pronounced effect on developing micro- and mesopore structures in pyrolysis compared to KOH. Activated char derived from $ZnCl_2$-impregnated SS *via* pyrolysis at 650 °C exhibited the highest S_{BET} of 54.1 $m^2 \cdot g^{-1}$ and V_{tot} of 0.539 $cm^3 \cdot g^{-1}$, along with a pyrolysis gas yield of 115.2 $ml \cdot g^{-1}$. The structural advantages translated into good performance as an adsorbent for MB removal. The findings provided valuable insights into efficient SS treatment strategies, enabling simultaneous recovery of high-value gas and activated char products.

CRediT Authorship Contribution Statement

Yuwen Zhu: Writing – review & editing, Writing – original draft, Funding acquisition, Data curation. Jian Liu: Software, Methodology, Investigation. Ting Li: Software, Methodology, Investigation. Xinrui Su: Methodology, Investigation. Qian Dai: Supervision, Methodology, Investigation. Chang Xu: Methodology, Investigation. Xuening Zhao: Methodology, Investigation. Hanqiao Liu: Supervision, Investigation.

Declaration of Competing Interest

The authors declare that they have no known competing financial interests or personal relationships that could have appeared to influence the work reported in this paper.

Acknowledgements

This work was financially supported by the National Natural Science Foundation of China (U21A2062) and National innovative training program for college students of China (202410792014).

Data Availability

Data will be made available on request.

Supplementary Material

Supplementary data related to this article can be found at https://doi.org/10.1016/j.cjche.2025.04.008.

References

[1] S. Guo, X.Y. Xiong, D.Y. Che, H.P. Liu, B.Z. Sun, Effects of sludge pyrolysis temperature and atmosphere on characteristics of biochar and gaseous products, *Kor. J. Chem. Eng.* 38 (1) (2021) 55–63.
[2] S.R. Naqvi, R. Tariq, M. Shahbaz, M. Naqvi, M. Aslam, Z. Khan, H. MacKey, G. McKay, T. Al-Ansari, Recent developments on sewage sludge pyrolysis and its kinetics: resources recovery, thermogravimetric platforms, and innovative prospects, *Comput. Chem. Eng.* 150 (2021) 107325.
[3] P. Feng, Y.X. Zhang, Z.Q. Xu, The effect of sludge from coal to oil process on the stability of coal/sludge water slurries, *Energy Sources Part A Recovery Util. Environ. Eff.* 40 (13) (2018) 1621–1628.
[4] K. Jayaraman, I. Gökalp, Pyrolysis, combustion and gasification characteristics of miscanthus and sewage sludge, *Energy Convers. Manag.* 89 (2015) 83–91.
[5] R. Toczyłowska-Mamińska, Limits and perspectives of pulp and paper industry wastewater treatment–A review, *Renew. Sustain. Energy Rev.* 78 (2017) 764–772.
[6] Y. Liang, D.H. Xu, P. Feng, B.T. Hao, Y. Guo, S.Z. Wang, Municipal sewage sludge incineration and its air pollution control, *J. Clean. Prod.* 295 (2021) 126456.
[7] Z.Y. Jin, F.M. Chang, F.L. Meng, C.P. Wang, Y. Meng, X.J. Liu, J. Wu, J.E. Zuo, K.J. Wang, Sustainable pyrolytic sludge-char preparation on improvement of closed-loop sewage sludge treatment: characterization and combined *in situ* application, *Chemosphere* 184 (2017) 1043–1053.
[8] S.Q. Tang, S.C. Tian, C.M. Zheng, Z.T. Zhang, Effect of calcium hydroxide on the pyrolysis behavior of sewage sludge: reaction characteristics and kinetics, *Energy Fuels* 31 (5) (2017) 5079–5087.
[9] S. Shahraki, M. Miri, M. Motahari-Nezhad, Experimental analysis of pyrolysis of sewage sludge, *Energy Sources Part A Recovery Util. Environ. Eff.* 40 (17) (2018) 2037–2043.
[10] H.L. Chiang, K.H. Lin, H.H. Chiu, Exhaust characteristics during the pyrolysis of $ZnCl_2$ immersed biosludge, *J. Hazard. Mater.* 229-230 (2012) 233–244.
[11] M. Inguanzo, A. Domınguez, J.A. Menéndez, C.G. Blanco, J.J. Pis, On the pyrolysis of sewage sludge: the influence of pyrolysis conditions on solid, liquid and gas fractions, *J. Anal. Appl. Pyrolysis* 63 (1) (2002) 209–222.
[12] F.M. Chang, C.P. Wang, Q.B. Wang, J.W. Jia, K.J. Wang, Pilot-scale pyrolysis experiment of municipal sludge and operational effectiveness evaluation, *Energy Sources Part A Recovery Util. Environ. Eff.* 38 (4) (2016) 472–477.
[13] Y.N. Chun, S.C. Kim, K. Yoshikawa, Pyrolysis gasification of dried sewage sludge in a combined screw and rotary kiln gasifier, *Appl. Energy* 88 (4) (2011) 1105–1112.
[14] M.A. Lillo-Ródenas, A. Ros, E. Fuente, M.A. Montes-Morán, M.J. Martin, A. Linares-Solano, Further insights into the activation process of sewage sludge-based precursors by alkaline hydroxides, *Chem. Eng. J.* 142 (2) (2008) 168–174.

[15] W.H. Li, Q.Y. Yue, B.Y. Gao, X.J. Wang, Y.F. Qi, Y.Q. Zhao, Y.J. Li, Preparation of sludge-based activated carbon made from paper mill sewage sludge by steam activation for dye wastewater treatment, *Desalination* 278 (1–3) (2011) 179–185.
[16] F. Rozada, M. Otero, A. Morán, A.I. García, Activated carbons from sewage sludge and discarded tyres: production and optimization, *J. Hazard. Mater.* 124 (1–3) (2005) 181–191.
[17] E. Raymundo-Piñero, P. Azaïs, T. Cacciaguerra, D. Cazorla-Amorós, A. Linares-Solano, F. Béguin, KOH and NaOH activation mechanisms of multiwalled carbon nanotubes with different structural organisation, *Carbon* 43 (4) (2005) 786–795.
[18] H. Chen, D.Z. Chen, L. Hong, Influences of activation agent impregnated sewage sludge pyrolysis on emission characteristics of volatile combustion and De-NO_x performance of activated char, *Appl. Energy* 156 (2015) 767–775.
[19] F. Li, B. Yan, Y.P. Zhang, L.H. Zhang, T. Lei, Effect of activator on the structure and desulphurization efficiency of sludge-activated carbon, *Environ. Technol.* 35 (17–20) (2014) 2575–2581.
[20] Y.H. Li, F.M. Chang, B. Huang, Y.P. Song, H.Y. Zhao, K.J. Wang, Activated carbon preparation from pyrolysis char of sewage sludge and its adsorption performance for organic compounds in sewage, *Fuel* 266 (2020) 117053.
[21] U. Mahapatra, A.K. Manna, A. Chatterjee, A critical evaluation of conventional kinetic and isotherm modeling for adsorptive removal of hexavalent chromium and methylene blue by natural rubber sludge-derived activated carbon and commercial activated carbon, *Bioresour. Technol.* 343 (2022) 126135.
[22] M. Saberi, P. Rouhi, Extension of the Brunauer-Emmett-Teller (BET) model for sorption of gas mixtures on the solid substances, *Fluid Phase Equilib.* 534 (2021) 112968.
[23] H. Chen, D.Z. Chen, Y.Y. Hu, Y.H. Feng, X.H. Dai, Preparation of activated sewage sludge char for low temperature De-NO_x and its CO emission inhibition, *Chemosphere* 251 (2020) 126330.
[24] G. Cheng, Y.Z. Li, L.M. Sun, S.Y. Luo, G.Z. Kyzas, J. Fu, Residue char derived from microwave-assisted pyrolysis of sludge as adsorbent for the removal of methylene blue from aqueous solutions, *Processes* 8 (8) (2020) 979.
[25] H.P. Yang, R. Yan, H.P. Chen, D.H. Lee, C.G. Zheng, Characteristics of hemicellulose, cellulose and lignin pyrolysis, *Fuel* 86 (12–13) (2007) 1781–1788.
[26] X. Li, G.Z. Wang, W.G. Li, Pyrolysis characteristics and kinetics of the preparation process of sludge-based activated carbon by $ZnCl_2$ activation method, *J. Harbin Inst. Technol.* 20 (6) (2013) 29–36.
[27] M. Wilk, A. Magdziarz, I. Kalemba, Characterisation of renewable fuels' torrefaction process with different instrumental techniques, *Energy* 87 (2015) 259–269.
[28] M. Olivares-Marín, C. Fernández-González, A. Macías-García, V. Gómez-Serrano, Preparation of activated carbon from cherry stones by chemical activation with $ZnCl_2$, *Appl. Surf. Sci.* 252 (17) (2006) 5967–5971.
[29] P.R. Dores-Silva, M.D. Landgraf, M.O.O. Rezende, Chemical differentiation of domestic sewage sludge and cattle manure stabilized by microbioreators: study by pyrolysis coupled to gas chromatography coupled to mass spectroscopy, *J. Braz. Chem. Soc.* 26 (5) (2015) 860–868.
[30] J. Meng, L.L. Wang, X.M. Liu, J.J. Wu, P.C. Brookes, J.M. Xu, Physicochemical properties of biochar produced from aerobically composted swine manure and its potential use as an environmental amendment, *Bioresour. Technol.* 142 (2013) 641–646.
[31] Y.W. Zhu, Y.J. Wang, T.Y. Wang, H.Q. Liu, H.Y. Liu, M.R. Zang, One-step preparation of coal-based magnetic activated carbon with hierarchically porous structure and easy magnetic separation capability for adsorption applications, *J. Magn. Magn Mater.* 569 (2023) 170480.
[32] B. Royer, N.F. Cardoso, E.C. Lima, J.C. Vaghetti, N.M. Simon, T. Calvete, R.C. Veses, Applications of Brazilian pine-fruit shell in natural and carbonized forms as adsorbents to removal of methylene blue from aqueous solutions: kinetic and equilibrium study, *J. Hazard. Mater.* 164 (2–3) (2009) 1213–1222.
[33] D.D. Li, J.Q. Li, Q.B. Gu, S.X. Song, C.S. Peng, Co-influence of the pore size of adsorbents and the structure of adsorbates on adsorption of dyes, *Desalination Water Treat.* 57 (31) (2016) 14686–14695.
[34] Q. Li, Y.J. Wang, R.T. Zhu, J.C. Wu, W.J. Zhang, H.Z. Lu, Rapid preparation of porous carbon by flash joule heating from bituminous coal and its adsorption mechanism of methylene blue, *Colloids Surf. A Physicochem. Eng. Aspects* 682 (2024) 132900.
[35] G.Q. Gong, S.J. Liang, Y.M. Shi, Z.Y. Wang, Z.L. Li, R.N. Li, S. Lu, Y.J. Zhang, Preparation of microporous carbon materials using residual coal from oxidative degradation of lignite as the carbon source and the mechanism and dynamics of its methyl orange adsorption, *Colloids Surf. A Physicochem. Eng. Aspects* 636 (2022) 128138.
[36] P. Kowalczyk, A.P. Terzyk, P.A. Gauden, G. Rychlicki, Numerical analysis of the Horvath–kawazoe equation: the adsorption of nitrogen, argon, benzene, carbon tetrachloride and sulphur hexafluoride, *Adsorpt. Sci. Technol.* 20 (3) (2002) 295–305.
[37] W. Plazinski, W. Rudzinski, A. Plazinska, Theoretical models of sorption kinetics including a surface reaction mechanism: a review, *Adv. Colloid Interface Sci.* 152 (1–2) (2009) 2–13.